AIAA SciTech Forum
8-12 January 2024, Orlando, FL
AIAA SCITECH 2024 Forum

10.2514/6.2024-0928

Control of Artificially-Generated Hairpin Vortices in a Laminar Boundary Layer

John D.B. Wylie* and Michael Amitay†
Rensselaer Polytechnic Institute, Troy, New York, 12180

Experiments were conducted to investigate the use of coherent vortical structures for boundary layer re-energization in a laminar boundary layer. The structures were generated artificially in the form of a hairpin train using a synthetic jet actuator to ensure repeatability for assessing the control. The structures act as a proxy for naturally occurring large-scale motions found in turbulent boundary layers. The hairpin train was controlled by both a static pin and a jet-assisted surface-mounted actuator (JASMA), and the results were captured using particle image velocimetry (PIV). Planar PIV was used to run a parameter study on several actuator strengths, angles, and heights along the domain mid-plane. Stereoscopic PIV measurements conducted downstream were aggregated into a volume of data for further analysis of the control of one particular hairpin train generation case. It was found that both the passive control pin and the active control JASMA contribute turbulent kinetic energy and downwash downstream to increase mixing and momentum injection into the boundary layer.

I. Nomenclature

AR_p = pin aspect ratio, h_p/d
AR_{sj} = synthetic jet aspect ratio, l_{sj}/h_{sj}
C_{b_J} = JASMA blowing ratio, U_J/U_∞
$C_{b_{sj}}$ = synthetic jet blowing ratio, U_{sj}/U_∞
d = pin diameter
H = boundary layer shape factor
h_p = pin height
h_{sj} = synthetic jet orifice width
l_{sj} = synthetic jet orifice length
Q^* = Q-criterion level normalized by h_{sj} and U_∞
U = streamwise velocity component
U_J = velocity at the JASMA orifice
U_{sj} = velocity at the synthetic jet orifice
U_∞ = free stream velocity
V = vertical velocity component
V_ϕ = vertical velocity component phase-locked to the synthetic jet cycle
$\bar{V}$ = time-averaged vertical velocity component
W = spanwise velocity component
x = streamwise coordinate
x^* = normalized streamwise coordinate, x/h_{sj}
y = vertical coordinate
y^* = normalized vertical coordinate, y/δ
z = spanwise coordinate
z^* = normalized spanwise coordinate, z/h_{sj}

---

[*] Graduate Student; Department of Mechanical, Aerospace, and Nuclear Engineering; 110 8th Street, Troy, NY.
[†] James L. Decker '45 Endowed Professor of Aerospace Engineering; Director, Center for Flow Physics and Control, 110 8th Street, Troy, NY. AIAA Fellow; Corresponding author, email: amitam@rpi.edu

α_{sj} = synthetic jet pitch angle
γ = JASMA pitch angle
δ = boundary layer thickness at $U/U_\infty = 0.99$
δ^* = boundary layer displacement thickness
θ = boundary layer momentum thickness
ν = kinematic viscosity
ϕ_J = JASMA phase angle
ϕ_{sj} = synthetic jet phase angle
ω_z = spanwise vorticity
ω_z^* = normalized spanwise vorticity, $\omega_z h_{sj}/U_\infty$

II. Introduction

Turbulent boundary layers contain coherent structures that possess significant turbulent kinetic energy (TKE). Typically, these large-scale motions (LSMs) reside in or at the edge of the boundary layer, leading to turbulent bulges at the edge [1]. These LSMs have a strong potential to re-energize the boundary layer if they were to be entrained near the surface. Agglomerations of LSMs, or very large-scale motions (VLSMs), contain roughly half of the Reynolds shear stresses in fully-developed turbulent boundary layer (TBL) flows [2]. In addition, these LSMs of size on the scale of the boundary layer thickness, $O(\delta)$, lead to increased smaller scale interactions [3], and the TBL outer layer motions are not unrelated to inner layer interactions as was previously thought. Researchers have proposed theoretical TBL models, summarized in [4], where LSMs are composed of trains of hairpin vortices convecting in close succession and interacting to generate prototypical TBL behaviors (e.g., sweeps and ejections). Hairpin vortices are thought to autonomously generate additional hairpins upstream, traveling in packets as LSMs [5, 6]. As such, control of hairpin vortices and other coherent structures in TBLs is of particular importance for boundary layer re-energization, which has applications such as control of separated flows.

Before attempting to control the naturally occurring hairpins in a TBL environment, it is prudent to establish a control scheme for the entrainment of these turbulent structures. The present work demonstrates control of artificially-generated hairpin vortices in a laminar boundary layer (LBL) environment. The LBL is chosen as a simpler analog to the TBL where suitable control can be developed in a regular and repeatable fashion.

A. Generation of Artificial Hairpin Vortices

Several works in literature have generated repeatable and periodically occurring hairpin vortices through both passive and active control methods. Active flow control refers to flow control methods requiring a supply of energy not present in the flow environment. Passive flow control on the other hand typically uses static structures such as fins/vortex generators, roughness elements, or bumps that require no energy to operate at the cost of being permanently situated in the flow environment. Acarlar and Smith [7] demonstrated repeatable hairpin formation via the shedding from hemispherical and teardrop-shaped bumps in a water tunnel. The same authors also tested active control methods such as steady fluid injection from a series of slots. They generated hairpin vortices with the shedding from a synthetic streamwise streak created by these slots [8]. An impulse-based fluidic injection was used by Haidari and Smith [9] to generate single hairpin vortices and observe the auto-generation process of child hairpins. Though less practical for devising hairpin-generating actuators, Taira and Colonius [10] showed that hairpin vortices are periodically shed from high angle of attack flat plates of low aspect ratio. Suponitsky et al. [11] fundamentally demonstrated that large amplitude disturbances in a laminar shear flow evolve into hairpin vortices, especially when inclined at a 45° angle. Works such as Van Buren et al. [12] have investigated the effect of various skew and pitch angles for high aspect ratio rectangular synthetic jets (SJs) in an LBL. Their results show two counter-rotating streamwise vortices in time-averaged flow fields and trains of vortex pairs resembling hairpin vortices in phase-locked frames. Studies like that of Jabbal and Zhong [13] have shown similar results using circular orifice geometries. Similar tests have also been conducted in the turbulent regime (e.g., [14]). Comprehensive numerical studies have been performed as well such as the systematic study by Zhou and Zhong [15] on the effect of stroke length and blowing ratio for a synthetic jet with a circular orifice for LBL flows. The present work investigates hairpins emanating from a rectangular synthetic jet orifice in an LBL.

B. Control and Entrainment of Coherent Structures

Since the LSMs often reside at $y \approx \delta$, flow control elements applying downwash to the structures are most applicable for boundary layer re-energization. Finite aspect-ratio cantilevered circular cylinders, or pins, are a static flow control method known for creating downwash and circulation in the wake region between a pair of counter-rotating tip vortices [16]. The flow features such as the separation bubble on the flat top and the flow fields around these pins are largely dependent on aspect ratio and Reynolds number. Numerous studies have defined these flow patterns for a large number of pin aspect ratios (e.g., [17–19]), and various cross-sectional shapes have been investigated [20]. Von Kármán vortex shedding is absent for pins below a critical aspect ratio depending on the immersion of the pin in the TBL [21]. Lower aspect ratio pins, such as the pin in the current work ($AR_p = 0.25$) are instead dominated by the arch vortex in the wake.

Other works have explored the destruction of LSMs in TBLs for achieving skin friction drag reduction. Spinosa [22] used synthetic jets to disrupt the large-scale motions, leading to a decrease in skin friction drag. The same work also investigated the interaction of an upstream synthetic jet with the streamwise streaks generated in the wake of a static pin. In contrast, this work uses a constructive interaction between the control actuator and the LSMs for momentum injection in the near-wall region of the boundary layer.

The present study utilizes a combination of control elements: low aspect ratio static pins and jet-assisted surface-mounted actuators (JASMAs). The JASMAs were conceived by Amitay and Gildersleeve [23] and were investigated with several pitch and skew angle configurations in both laminar and turbulent boundary layers ([24] and [25]). They showed that JASMAs introduce increased downwash in the wake of the cantilevered pin.

A limited number of works have demonstrated control of LSMs and hairpin vortices for this purpose. Tsolovikos et al. [26] used model predictive optimal control to identify TBL LSMs in a control region and actuation from a Gaussian ellipsoid forcing region to apply downwash to the structures. Their direct numerical simulations showed that vorticity fluctuations near the wall increased most when the structures were controlled (as opposed to when the structures were present independently) across several streamwise stations downstream. Jariwala et al. [27] generated and controlled hairpin trains in an LBL using an upstream-pointed, Gaussian forcing region and subsequent downward forcing resembling that of a plasma actuator. To build on these works and provide experimental evidence of these concepts, this work proposes an experimental methodology for controlling synthetic hairpin vortices and other vortical structures using either a cantilevered pin or a JASMA.

The present work has applications to separation control and other benefits of boundary layer re-energization. Rather than utilizing traditional control strategies, the current work attempts to reap the high TKE from existing turbulent structures using weaker control elements to entrain them into the inner region of the LBL flow. Such control should reduce the required amount of energy expenditure compared to indiscriminate active control such as steady blowing or suction. Furthermore, choosing active or hybrid control techniques over fully passive alternatives permits flexibility in varying flow scenarios.

III. Experimental Setup and Procedure

This section describes the details of the wind tunnel experiments conducted to explore the effect of two flow control techniques on artificially-generated hairpins for boundary layer re-energization. Stereoscopic particle image velocimetry measurements were used to explore the volumetric flow fields. The experiments were performed in the low-speed suction wind tunnel at the Center for Flow Physics and Control at Rensselaer Polytechnic Institute. The tunnel test section has a cross-section of 101.6 mm × 101.6 mm and is 508 mm long. The test section floor has a cutout for flush-mounting various test modules.

A. Model Setup

The present experiments were conducted using multiple module configurations with an upstream synthetic jet and either a cantilevered circular pin or a JASMA located downstream of the synthetic jet with a center-to-center distance of 38.3 mm (12.9δ, where δ is the boundary layer thickness just upstream of the synthetic jet orifice). The experiments were conducted with various synthetic jet pitch angles and blowing ratios, pin heights, and JASMA pitch angles and blowing ratios.

The hairpin vortices were generated using a synthetic jet with a rectangular orifice (dimensions of $l_{sj} \times h_{sj} = 12$ mm × 1 mm). Two pitch angles were tested: $\alpha_{sj} = 45°$ and 90° (see Figure 1). Both jets were tested at blowing ratios of $C_{b_{sj}} = 0.5$ and 1. A cantilevered circular pin module insert with a diameter of $d = 12$ mm and heights of 2, 3, or 4 mm (corresponding to $h_p/\delta = 0.67$, 1.0 and 1.33 and aspect ratios of $AR_p = 0.167$, 0.25 and 0.33) was placed 38.3 mm downstream of the synthetic jet. Spacers were used to adjust the pin height and could be used to achieve a flush configuration for the generation of artificial hairpin trains without downstream control. Another module insert, consisting of the JASMA, was positioned instead of the pin with its orifice facing downstream. Two JASMA inserts were tested with pitch angles of $\gamma = 0°$ and $-20°$. The synthetic jet orifice on the JASMAs had a cross-section of 6 mm × 0.5 mm, maintaining the same aspect ratio as that of the synthetic jet orifice ($AR_{sj} = 12$). The wind tunnel modules were designed such that the JASMA insert was removable to vary the pitch angle as needed. The two modules were manufactured using the stereolithography (SLA) process with Accura ABS Black (SL 7820). Both the SJ and JASMA were driven with sinusoidal waveforms at a frequency of 1.10 kHz, which was chosen as an off-resonance frequency.

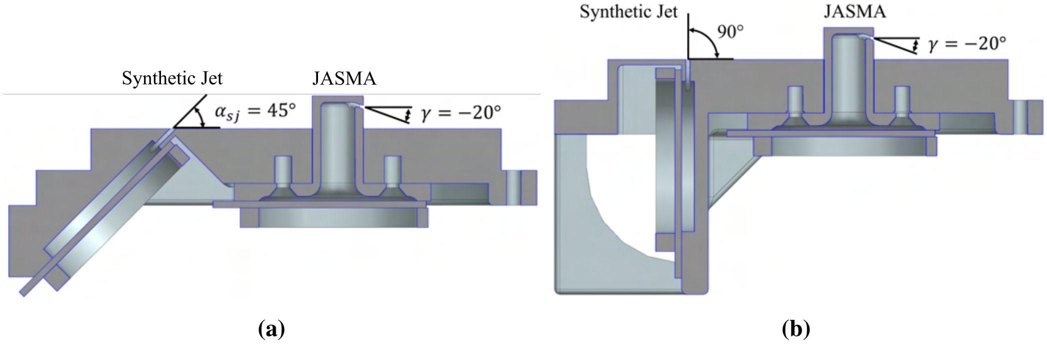

Fig. 1 Sectional views of the wind tunnel modules for synthetic jet pitch angles of $\alpha_{sj} = 45°$ (a) and 90° (b). The JASMA is removable and separate inserts are used for $\gamma = 0°$, $\gamma = -20°$, and the cantilevered pin.

At the location of the synthetic jet, the incoming flow had a boundary layer thickness of $\delta = 2.98$ mm, a displacement thickness of $\delta^* = 0.98$ mm, a momentum thickness of $\theta = 0.36$ mm, and a shape factor of $H = 2.71$. The baseline boundary layer was compared to the Blasius profile to validate that the boundary layer is laminar (not shown here for brevity).

B. Planar Particle Image Velocimetry

To compare the effects of individual parameters (i.e., synthetic jet or JASMA pitch angle and blowing ratio as well as pin height), numerous planar particle image velocimetry (2D PIV) test cases were tested along the centerline ($z^* = 0$) of the flow field (Figure 2a). The full list of test cases is shown in the Appendix in Table 1. For brevity, only a number of cases are included here. A few configurations were chosen based on these results to be fully characterized by stereoscopic particle image velocimetry.

2D PIV images were acquired using a 2 MP LaVision Imager Pro X CCD camera. Water-glycol seed particles with a mean diameter $O(1\ \mu m)$ were dispersed upstream of the tunnel and seeded into the test section for uniform coverage. The particles were illuminated with a 120 mJ New Wave Nd:YAG double-pulsed laser. The incident ray was focused using an adjustable focal lens (focal length from 500 to 3000 mm) and fanned into a sheet using a cylindrical lens (radius of -20 mm). A 100 mm Tokina lens was used to visualize a domain of 82.9 mm × 62.2 mm while the camera was oriented along the spanwise axis normal to the interrogation plane of interest. The DaVis 8.4.0 software from LaVision GmbH communicated with a programmable timing unit to synchronize the lasers, the image acquisition, and the synthetic jet actuation.

For all PIV experiments, 250 image pairs were acquired for time-averaged and phase-locked cases to achieve convergence of the mean velocity and RMS fields. The image pairs were processed using a double-exposure image cross-correlation algorithm with interrogation windows of decreasing size: first with one pass of 32 pixels × 32 pixels windows and then with two passes of 16 pixels × 16 pixels, both with 50% overlap. The resulting vector field had a resolution of 1.21 vectors/mm. The velocity vectors were post-processed with outlier detection and masked to remove laser reflection and surface regions. Baseline flow fields were matched with the Blasius solution to determine the correct location of the surface. For this work, the streamwise coordinate is normalized by the width of the synthetic jet, $h_{sj} = 1$ mm. The vertical coordinate is normalized by the boundary layer thickness, δ, of the baseline flow field just upstream of the synthetic jet orifice, and all velocities are normalized by the free stream velocity. All normalized parameters are written as starred variables (e.g., $x^* = x/h_{sj}$).

C. Stereoscopic Particle Image Velocimetry

Three-component stereoscopic particle image velocimetry (SPIV) was used to further quantify and visualize the artificially-generated hairpin vortices and the effect of the downstream control. An additional camera and lens pair was added and both were retrofitted with Scheimpflug lens adapters. The cameras were oriented on both sides of the test section facing upstream as shown in Figure 2b to view streamwise-normal planes. Each SPIV vector field covered a region of 50.7 mm × 28.6 mm. The cameras and laser were traversed consistently each by three Velmex slide traverses with Vexta PK296 motor traverses. To obtain the flow field of interest, the laser plane and cameras were shifted in the streamwise direction to acquire a total of 41 planes starting at $x/h_{sj} = 50$ and moving downstream at a spacing of 1 mm. As such, the full domain included planes in the range of $x/h_{sj} = [50, 90]$. At each plane, a minimum of 250 image pairs were acquired. The disparity vector between camera focal and laser planes was corrected at each spanwise-normal plane using an SPIV self-calibration algorithm. The vector fields for all planes were post-processed by combining the planes, linearly interpolating to a common three-dimensional grid, and smoothing via a three-dimensional convolution. The full list of test cases for the SPIV data volume is shown in the Appendix in Table 2.

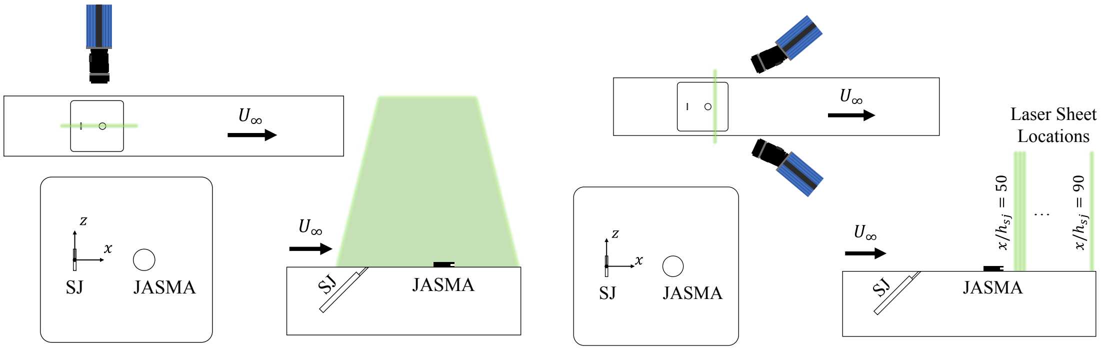

(a) **(b)**

Fig. 2 Wind tunnel PIV (a) and SPIV (b) setups. The upstream synthetic jet issues from the test section floor into the crossflow. The JASMA is located downstream of the synthetic jet.

IV. Results and Discussion

This section discusses the results of the experimental campaign to generate and control artificial, coherent vortical trains in a laminar boundary layer. First, selected results highlight the parametric study to determine the actuation case for a volumetric analysis. These are presented in the form of planar PIV results. Then, SPIV volumes for the generation and control cases of interest are analyzed in more detail.

A. Planar Particle Image Velocimetry

The effects of various parameters on the generation of hairpins, namely the synthetic jet pitch angle, α_{sj}, and blowing ratio, $C_{b_{sj}}$, were measured and compared along the centerline. In addition, the control of the hairpin vortices farther downstream was explored using a cantilevered circular pin or JASMA.

The generation of the hairpin vortices is discussed first. Figure 3 presents color contours of mean-subtracted phase-locked wall-normal velocity, superimposed with in-plane velocity vectors, for four combinations of blowing ratios and pitch angles of the synthetic jet. This method of subtracting the time-averaged flow field changes the inertial frame of reference, which was also utilized by Adrian et al. [28] and others for better hairpin identification. Note that $x^* = 0$ corresponds to the center of the synthetic jet orifice. Green arrows are shown to visualize synthetic jet pitch angle, α_{sj}, and blowing ratio, $C_{b_{sj}}$.

All cases in Figure 3 show a train of vortices that remain coherent through the domain but with diminishing strength. The case of interest chosen was the synthetic jet with $C_{b_{sj}} = 0.5$ and $\alpha_{sj} = 45°$. This case generated coherent structures that resided just outside the boundary layer and convected close to the free stream velocity ($U/U_\infty \approx 0.98$ for $\alpha_{sj} = 45°$ compared to ≈ 0.88 for $\alpha_{sj} = 90°$). The case where the synthetic jet was pitched at $\alpha_{sj} = 90°$ resulted in deeper penetration into the crossflow, a deceleration of a larger region of fluid, and a slower streamwise convective velocity.

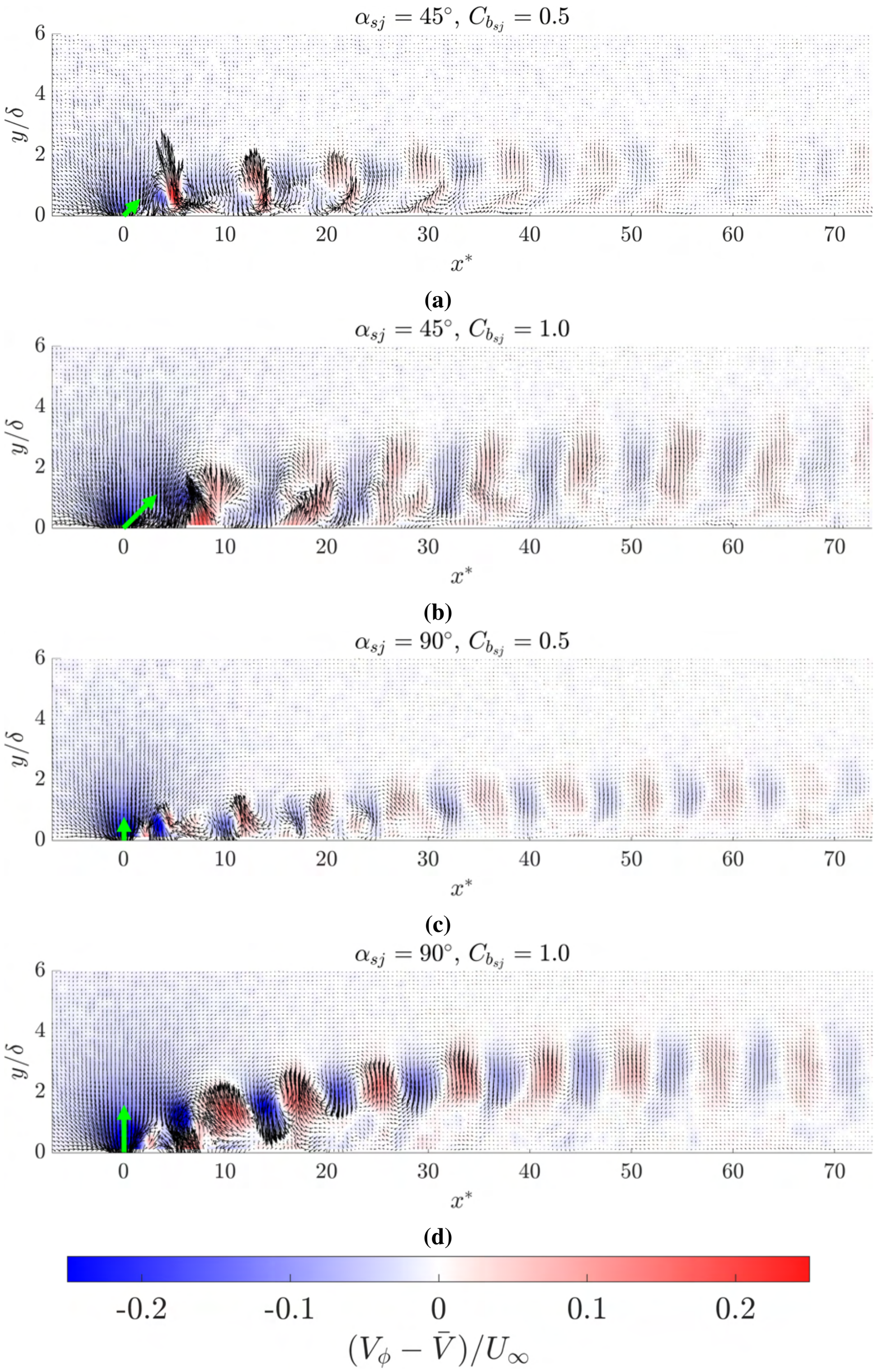

(a)

(b)

(c)

(d)

Fig. 3 Color contours of mean-subtracted phase-locked wall-normal velocity, superimposed with in-plane velocity vectors, for synthetic jet pitch angles $\alpha_{sj} = 45°$ (a and b) and $90°$ (c and d) and blowing ratios $C_{b_{sj}} = 0.5$ (a and c) and 1.0 (b and d). Flow is from left to right.

As mentioned previously, two control techniques were explored, the cantilevered pin and the JASMA. Before exploring their effect on the train of artificially-generated hairpin vortices, the interaction of each of them with the laminar boundary layer (in the absence of the hairpins) is presented. The effect of the pin's height, with respect to the local boundary layer thickness, is presented in Figure 4. Figure 4 shows color contours of the normalized streamwise velocity with in-plane velocity vectors for $h_p/\delta = 0.67$ (a), 1.0 (b), and 1.34 (c). Note that only every fourth column of velocity vectors is shown for visual clarity.

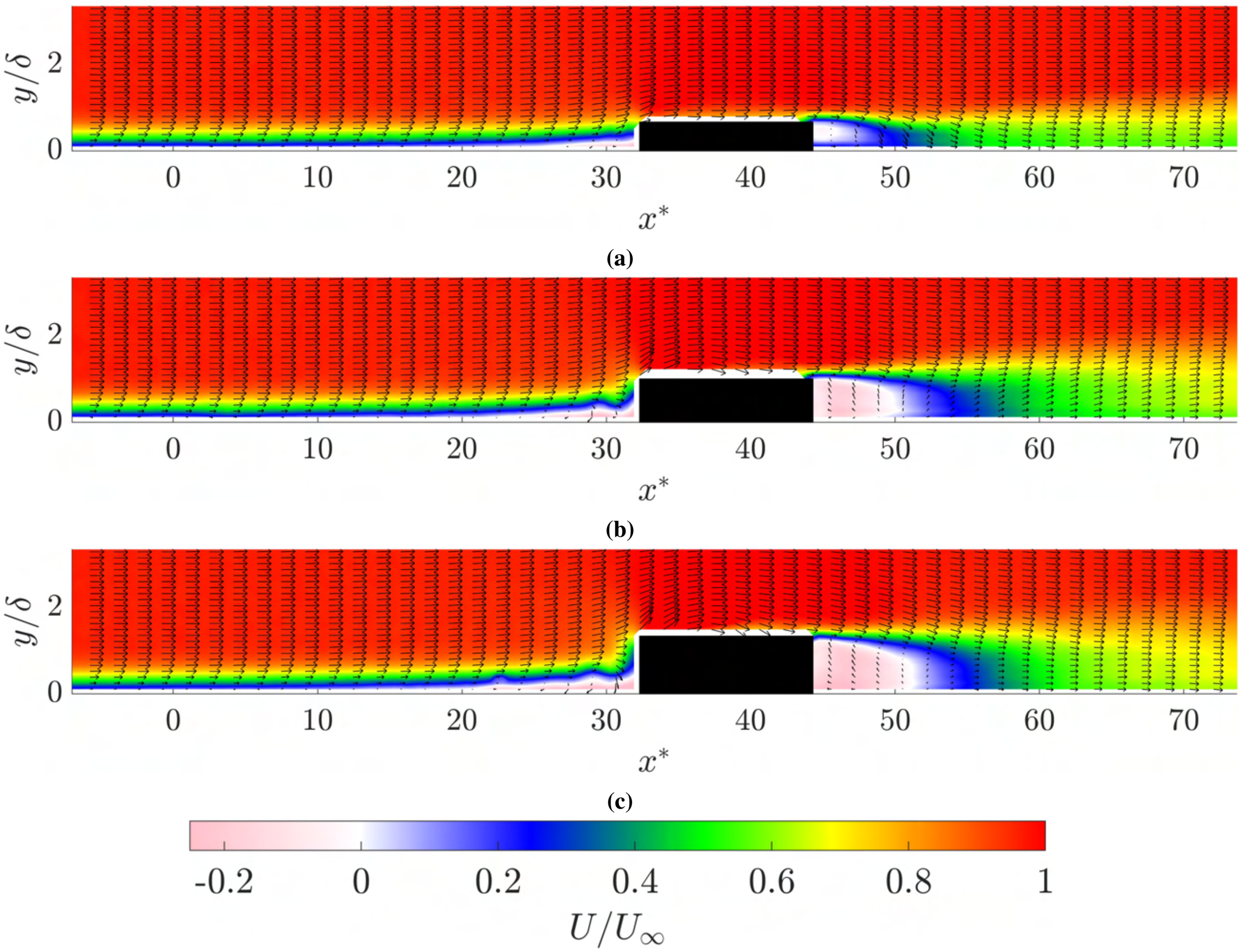

(a)

(b)

(c)

Fig. 4 Color contours of the normalized streamwise velocity with in-plane velocity vectors for $h_p/\delta = 0.67$ (a), 1.0 (b), and 1.34 (c). Flow is from left to right.

As can be seen, in all cases, the flow field along the centerline ($z^* = 0$) contains a region of reversed flow behind the pin and downwash, followed by a decelerated mean flow. As expected, the size of the separation bubble increases with increasing pin height. Moreover, the undulation of the mean flow just upstream of the pin suggests the presence of horseshoe vortices. As was shown by Gildersleeve and Amitay [19], the number of horseshoe vortices and their size are directly related to the relative height of the pin. In the present paper, the case where the relative pin height is $h_p/\delta = 1.0$ was chosen as an intermediate between maximizing downwash and minimizing blockage.

Next, the interaction of the JASMA with the laminar boundary layer is explored for a relative pin height of $h_p/\delta = 1.0$ and a blowing ratio of $C_{b_J} = 0.5$ at two JASMA pitch angles as shown in Figure 5. As in the previous phase-locked flow field, color contours of the normalized, time-average-subtracted, phase-locked wall-normal velocity are shown superimposed with in-plane velocity vectors. Again, green arrows are shown to visualize α_{sj} and $C_{b_{sj}}$.

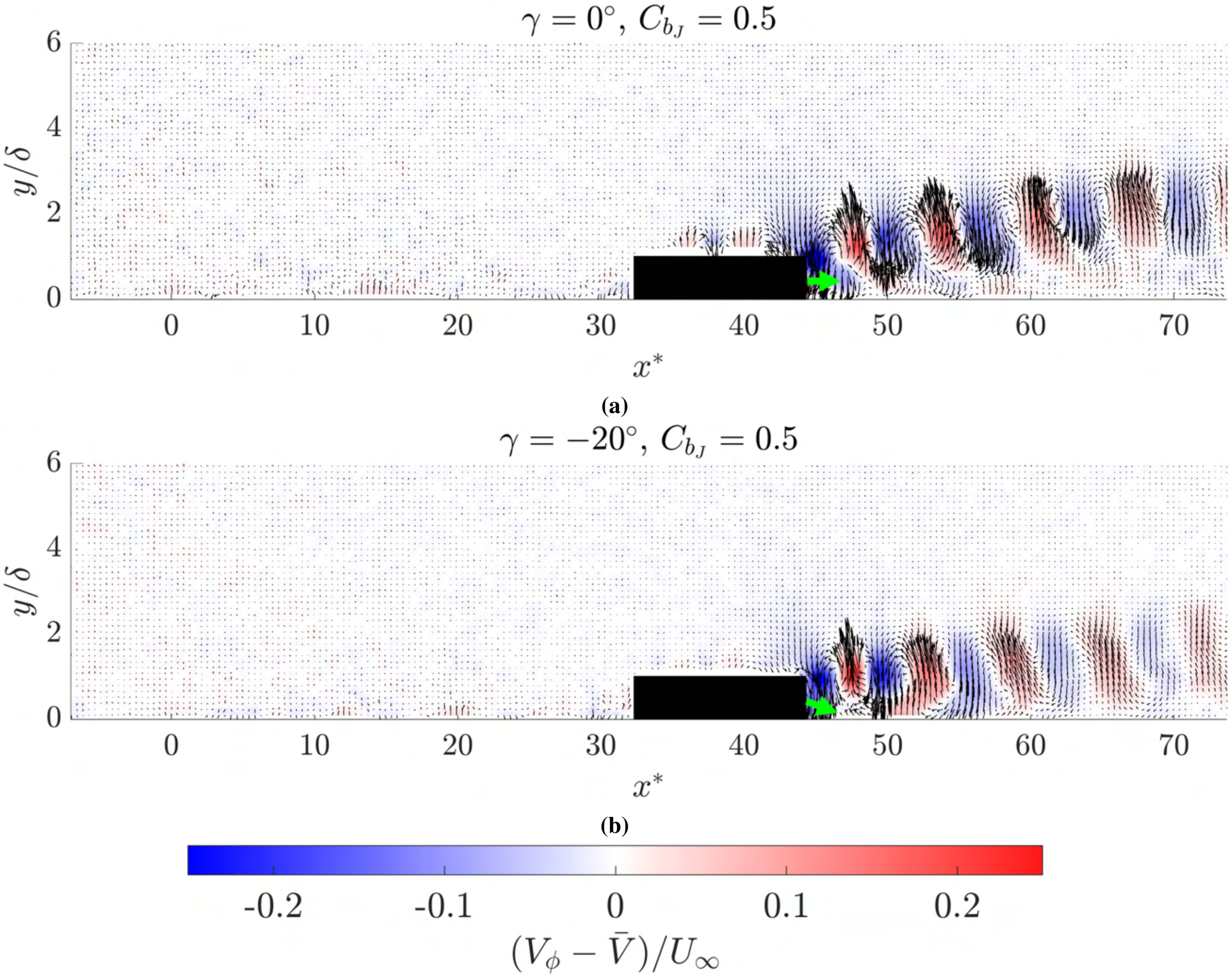

(a)

(b)

Fig. 5 Color contours of mean-subtracted phase-locked wall-normal velocity, superimposed with in-plane velocity vectors, for the JASMA pitch angles $\gamma = 0°$ (a) and $-20°$ (b). The relative pin height is $h_p/\delta = 1.0$ and the blowing ratio is $C_{b_J} = 0.5$.

For both pitch angles, a train of vortices is generated and advects downstream with diminishing strength. As can be seen, the induced vertical velocities from the vortical structures are weaker for the $\gamma = -20°$ case because the JASMA jet impinges on the plate. Moreover, this leads to a decreased convective velocity of the structures ($U/U_\infty \approx 0.64$ for $\gamma = -20°$ compared to $U/U_\infty \approx 0.72$ for $\gamma = 0°$). Therefore, the $\gamma = 0°$ case was chosen for further testing.

Once the synthetic jet, pin, and JASMA parameters were established, the effect of the pin and the JASMA on the hairpins' trajectory and strength was explored. Figures 6a-c present color contours of mean-subtracted phase-locked wall-normal velocity, superimposed with in-plane velocity vectors, for the synthetic jet-only, the synthetic jet with the cantilevered pin, and the synthetic jet with the JASMA, respectively. Again, green arrows are shown to visualize α_{sj} and γ.

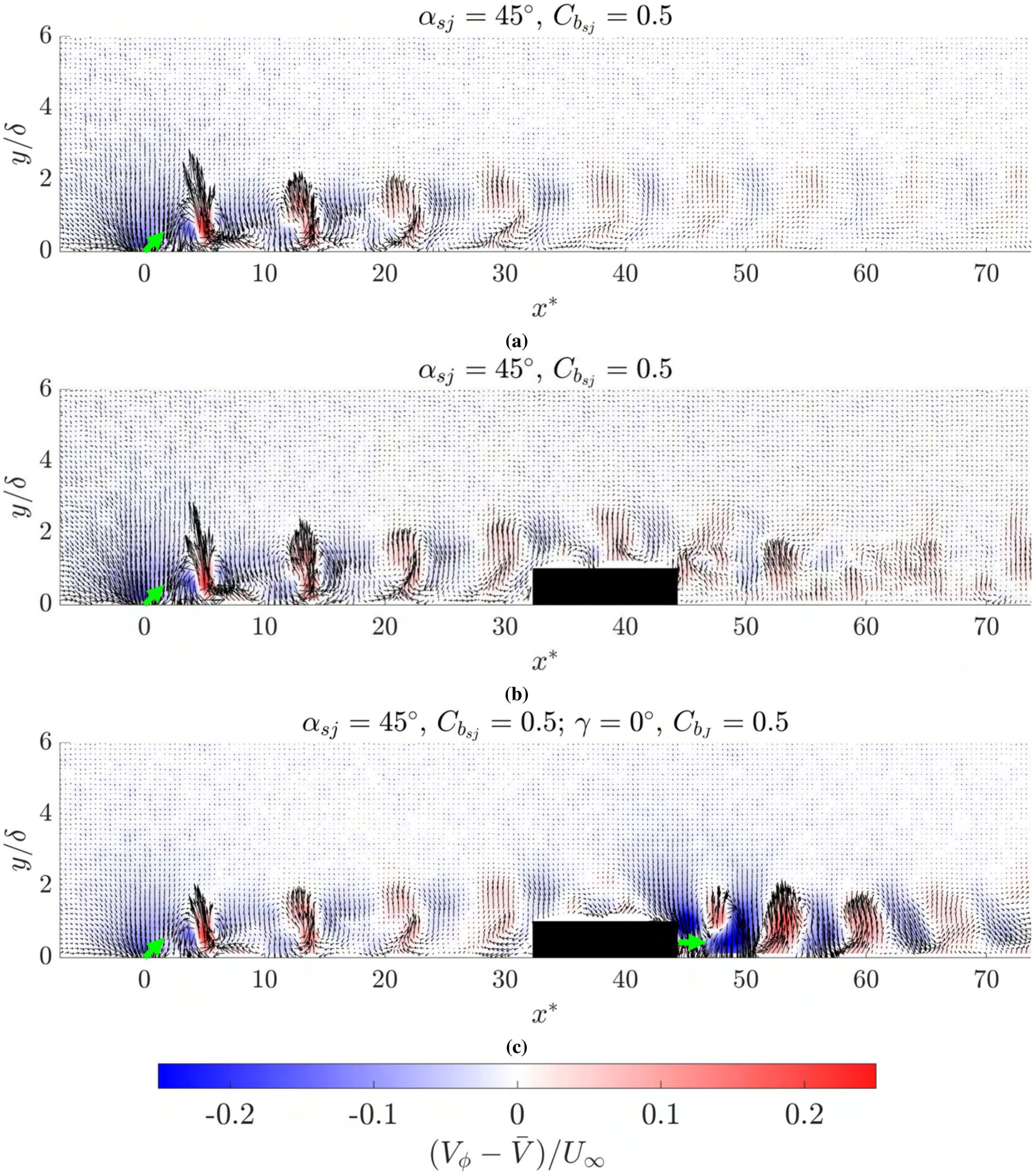

(a)

(b)

(c)

Fig. 6 Color contours of mean-subtracted phase-locked wall-normal velocity, superimposed with in-plane velocity vectors, for the synthetic jet-only (a), the synthetic jet with the static pin (b), and the synthetic jet with the JASMA (c). Flow is from left to right.

Comparing Figure 6a to Figure 6b clearly shows that the vortical structures are pulled towards the surface downstream of the pin due to the downwash induced by it. Comparing Figure 6a to Figure 6c shows that the interaction of the hairpin vortices with the JASMA results in the coherent structures (generated by the JASMA) residing closer to the surface. In addition, the JASMA increases downwash in the pin wake compared to the other cases in the near-wall portion of the boundary layer (6c).

B. Volumetric Flow Fields

Next, the volumetric SPIV results obtained for a particular actuator configuration with a synthetic jet pitched at 45° to the surface ($\alpha_{sj} = 45°$) and a blowing ratio of $C_{b_{sj}} = 0.5$ are discussed in detail. The coherent structures were manipulated by a static pin or a JASMA with height $h_p/\delta = 1$. The JASMA chosen had a synthetic jet orifice with $\gamma = 0°$ and a blowing ratio of $C_{b_J} = 0.5$. The time-averaged flow fields are first examined for the following cases: the synthetic jet alone, the static pin alone, the interaction of the synthetic jet with the downstream static pin, the JASMA alone, and the interaction of the synthetic jet with the downstream JASMA. These five cases are shown in Figure 7 as iso-surfaces of normalized vertical velocity with red indicating upwash and blue indicating downwash. Transparent iso-surfaces are overlaid at levels of $V/U_\infty = \pm 0.2, \pm 0.3, \pm 0.4, \pm 0.5$.

The case of the synthetic jet alone (Figure 7a) leads to faint regions of upwash near the domain centerline. As will be shown, these are due to the upwash induced by the counter-rotating hairpin vortex legs. The corresponding upwash outboard of the vortex legs is not seen since the contour levels are not small enough to capture that information.

The static pin-alone case (Figure 7b) contains regions of flow associated with several vortical features related to the pin: the horseshoe vortices, the arch vortex in the wake, and the separated shear layer over the top. The horseshoe vortices contribute by inducing downwash that constructively merges with that from the arch vortex, generating two prominent downwash regions that extend in the streamwise direction. For detailed flowfield measurements, see Gildersleeve and Amitay [19].

The first observation from examining the interaction between the SJ-generated hair pins and the static pin (Figure 7c) is the decrease in mid-plane upwash. Closer examination also reveals that the downwash is increased in strength compared to that of the static pin-alone case. This feature will be explored in more detail later.

The JASMA alone (Figure 7d) generates pronounced flow patterns. The structure of static pin wake is preserved, but the downwash regions are concentrated into more streamwise-oriented regions. Likewise, the upwash is emboldened. This will be shown in the phase-locked data presented later in this paper to be the effect of the strong hairpin vortices that are generated by the JASMA's synthetic jet. Again, the hairpin legs on each side of the mid-span plane induce positive vertical velocity in the mid-span while inducing vertical velocity in the opposite direction outboard of the vortices. Since the induced vertical velocities of the JASMA hairpin vortex train are aligned with those induced by the static pin vortices, the upwash and downwash regions are more prominent.

The interaction of the SJ-generated hairpins with the JASMA (Figure 7e) leads to a reformatted wake with decreased upwash. Note that the asymmetry is surmised to be due to slight flow field asymmetries in the individual actuator cases (i.e., the synthetic jet alone and the JASMA alone). This leads to a combined effect where the streamwise-oriented vertical velocity regions are tilted slightly in the positive z^* direction. As will be shown, the strengthened downwash in $z^* < 0$ aligns well with the goal of this work: to entrain coherent structures and induce mixing in the boundary layer.

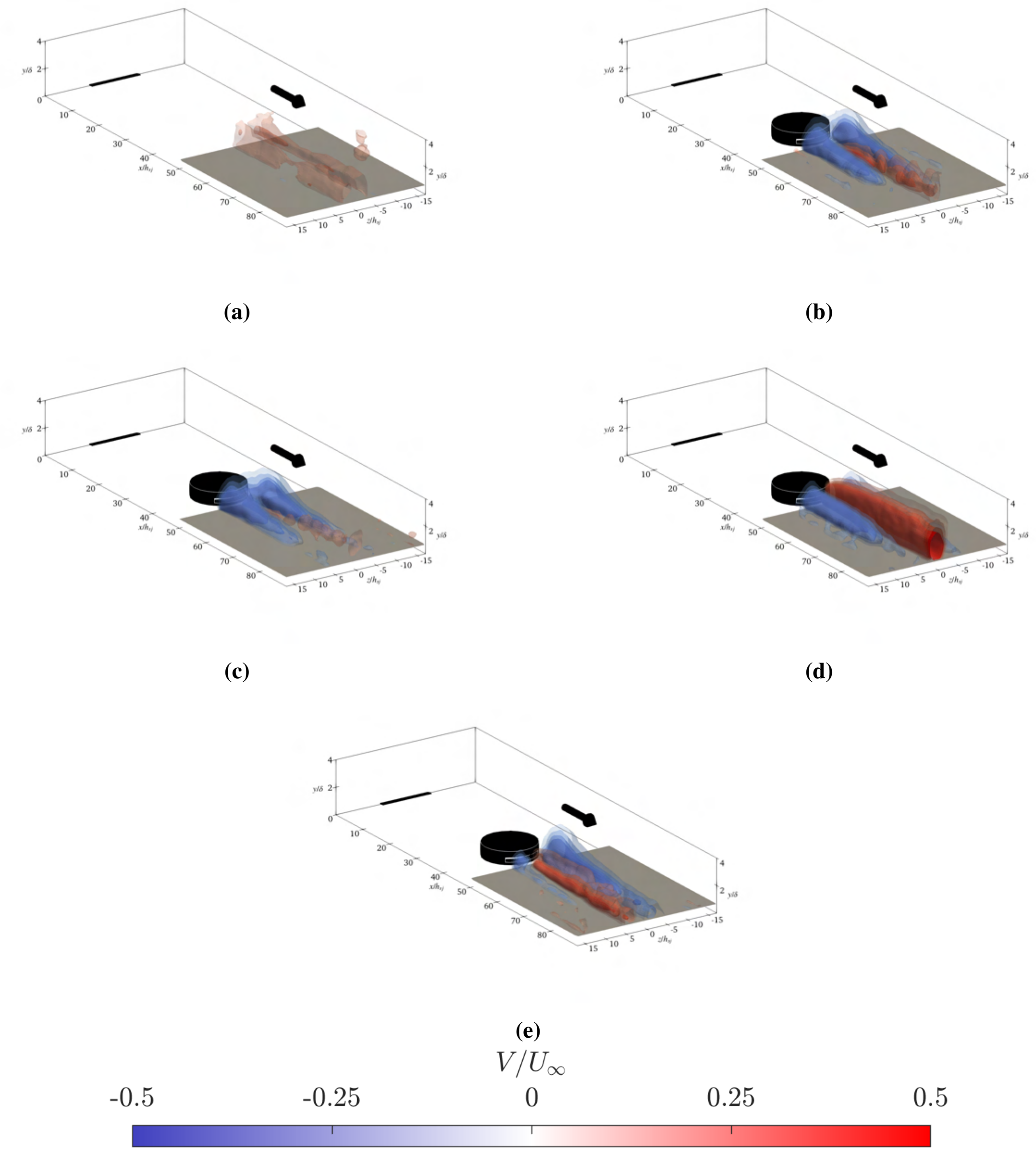

(a) (b) (c) (d) (e)

Fig. 7 Iso-surfaces of time-averaged, normalized vertical velocity at levels of $V/U_\infty = 0.2, 0.3, 0.4, 0.5$ **for the synthetic jet alone (a), static pin alone (b), synthetic jet with static pin (c), JASMA alone (d), and synthetic jet with JASMA (e).**

Clearly, between the pin wake shedding and the unsteady synthetic jet-based actuation, the flow phenomena are highly unsteady. To envision this behavior, phase-locked Q-criterion contours are presented at a common representative phase of the actuation cycle in Figure 8. The contours of Q^* are colored by normalized streamwise vorticity. The static pin-only case is omitted here since there is no actuation cycle or conditional sampling from which to phase lock the data.

For the generation case with the synthetic jet actuation alone (Figure 8a), a series of hairpin vortices are generated that convect downstream. The highest vortical content is depicted by the counter-rotating hairpin legs shown in red for $z^* > 0$ and blue for $z^* < 0$. The legs do not meet in this representation due to the choice of Q^* level, but the 2D PIV representation (Figure 3a) confirms that vortices denoting the hairpin heads are present on the mid-plane.

When the synthetic jet interacted with the static pin (Figure 8b), two sets of legs from the horseshoe vortices forming around the base of the pin are seen (blue for $z^* > 0$ and red for $z^* < 0$). The same hairpins are visualized between these horseshoe vortices. This indicates that the pin is not too intrusive in disrupting the hairpin train. In fact, the vorticity levels indicate that the pin has strengthened the hairpin train.

For the JASMA alone case (Figure 8c), narrower, coherent hairpins form downstream of the actuator in a similar train to those seen in Figure 8a. In this case, the hairpin legs connect to form strong vortices. These hairpins are the result of truncated vortex rings from the orifice. This is due to the proximity of the orifice to the floor and the smaller synthetic jet orifice.

The interaction of the SJ-generated hairpins with the JASMA-generated hairpins (Figure 8d) depicts a train of vortices that are more coherent in terms of Q^* than those of the SJ-alone case (Figure 8b). The vortices are tilted downstream, and closer to the surface.

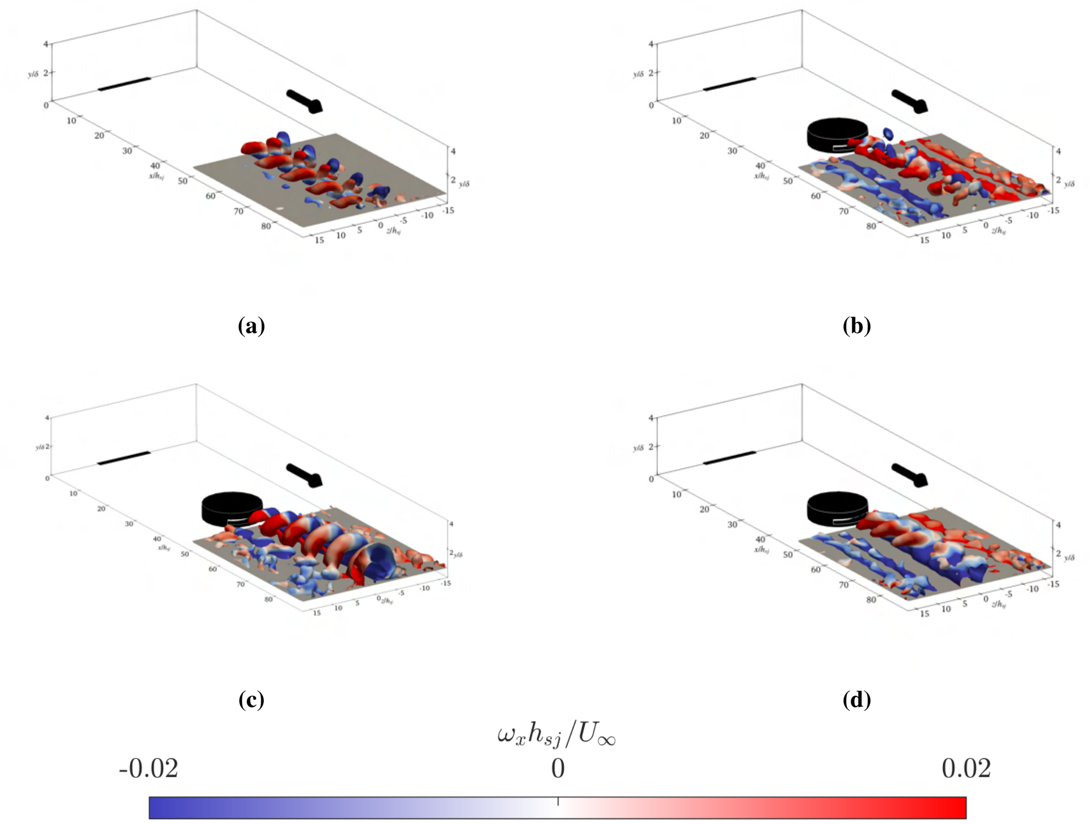
(a)

(b)

(c)

(d)

Fig. 8 Contours of normalized Q ($Q^* = 4.64 \times 10^{-4}$) colored by normalized streamwise vorticity for four cases: synthetic jet alone (a), synthetic jet with static pin (b), JASMA alone (c), and synthetic jet with JASMA (d).

Next, four phases along the actuation cycle of the synchronous synthetic jet and JASMA ($\phi_{sj} = \phi_J$) are shown in Figure 9. The vortices generated by the synthetic jet convect downstream and are locked to the JASMA actuation cycle once they pass the pin. The actuation also appears to cause the horseshoe vortex legs from the static pin to oscillate as indicated by the lobes. To determine the efficacy of the control, further quantification of the wake region is required.

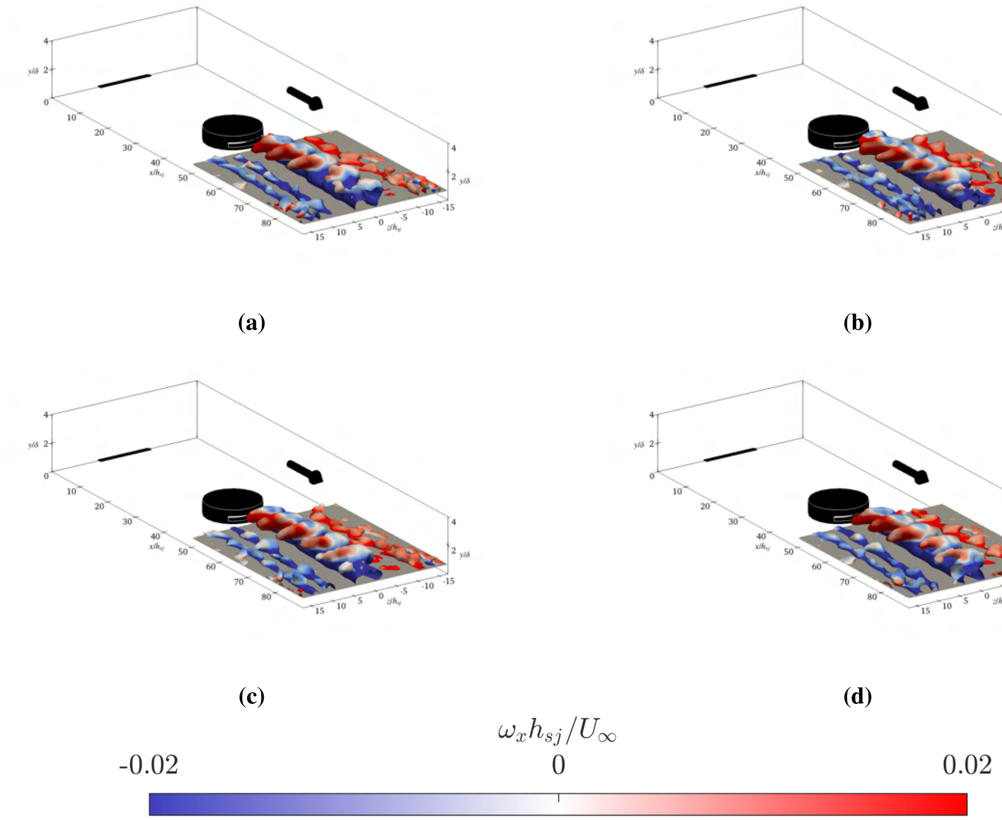

(a) **(b)** **(c)** **(d)**

Fig. 9 Contours of normalized, phase-locked Q ($Q^* = 4.64 \times 10^{-4}$) colored by normalized streamwise vorticity for four phases of the synthetic jet cycle: $\phi_{sj} = 0^\circ$ (a), 90° (b), 180° (c), and 270° (d).

Next, the normalized streamwise velocity contours at two spanwise planes downstream of the recirculation region of the pin wake at $x^* = 75$ and 85 are shown in Figure 10. The velocity contours are plotted for the same five cases presented in Figure 7. Spanwise undulations in the streamwise velocity for the synthetic jet alone case can be attributed to the streamwise streaks generated by the hairpin train legs. When the pin is present in the flow, a decelerated wake forms behind it. Two downstream locations were chosen downstream of the reversed flow region, but the flow has not fully recovered in terms of velocity magnitude. The case of the SJ with the static pin exhibits an increase in the near wall momentum around $z^* = \pm 6$. When only the JASMA is present in the flow, there is an additional streamwise momentum in the boundary layer from approximately $z^* = -7$ to 7. When the SJ and the JASMA are both present in the flow, a large region of momentum gains from approximately $z^* = -8$ to 2 with the wake region redirected to roughly $z^* = 2$ to 7. The momentum addition to the near wall region of the flow, as shown for the JASMA alone and SJ and JASMA together, is one of the desired outcomes of this work. It is expected that this will aid in the control of separated flows.

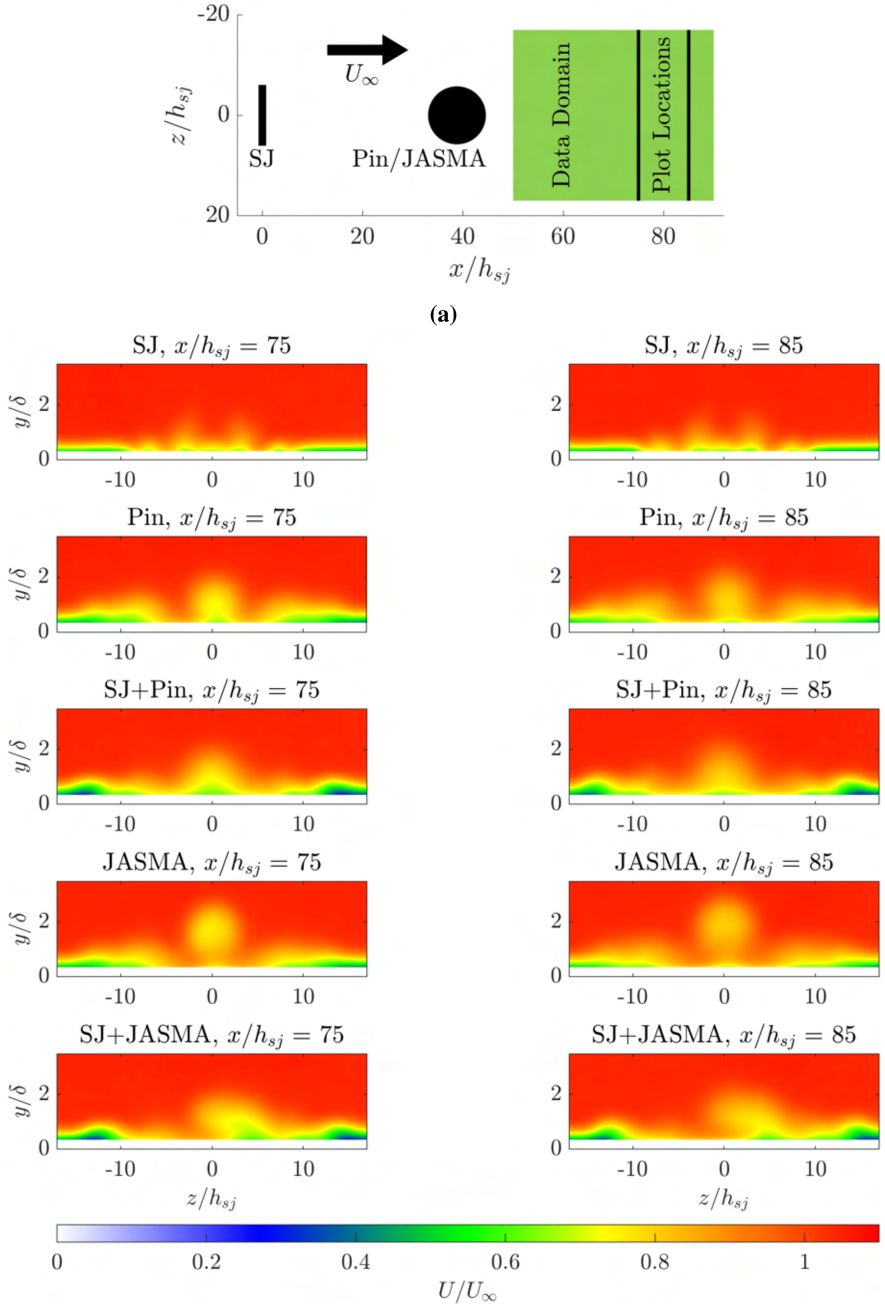

(a)

(b)

Fig. 10 Schematic representation of the experimental setup with data domain in green and contour locations shown by the solid black lines (a). Contours of normalized streamwise velocity at $x^* = 75$ (left column) and 85 (right column) for SJ-alone case (row 1), static pin-alone case (row 2), SJ and static pin case (row 3), JASMA-alone case (row 4), and SJ with JASMA case (row 5) (b). The mean flow direction is into the page.

To further quantify the effects of the pin and the JASMA on the SJ-generated hairpins, the wall-normal profiles of the vertical velocity at six locations in the wake are shown in Figure 11. The locations are chosen along the span at the same two streamwise stations shown in Figure 10. When only the synthetic jet is present in the flow, there is positive velocity (upwash) across most of the boundary layer with only a slight downwash in the near wall region of the boundary layer at some locations. The pin-alone, the SJ+pin, and the JASMA-alone cases increase the downwash compared to the SJ-alone case away from the centerline. However, near the centerline, these cases contribute to upwash.

The upwash for all of the above cases can be attributed to the induced upwash from the counter-rotating hairpin vortex legs. The large upwash from the JASMA-alone case near the mid-plane is exacerbated by the proximity of the JASMA orifice to the surface. This is consistent with the wake of the JASMA seen in Figure 5a. The disproportionately large JASMA contribution suggests that further refinement of the JASMA amplitude is necessary. Finally, when both the SJ and JASMA are present in the flow, downwash is generated in all regions shown, which is precisely the desired outcome. It is worth noting that when only the JASMA is present in the flow, the downwash slightly exceeds the case of the SJ and JASMA present together at $z^* = -4.16$, but this downwash is outweighed by the large upwash from the JASMA-alone case near the mid-plane. It is clear from the JASMA behavior that its interaction with the synthetic jet is highly nonlinear; moreover, the JASMA-alone and SJ-alone cases do not superpose to yield the SJ+JASMA case.

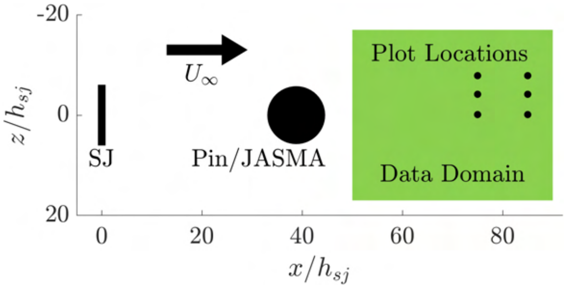

(a)

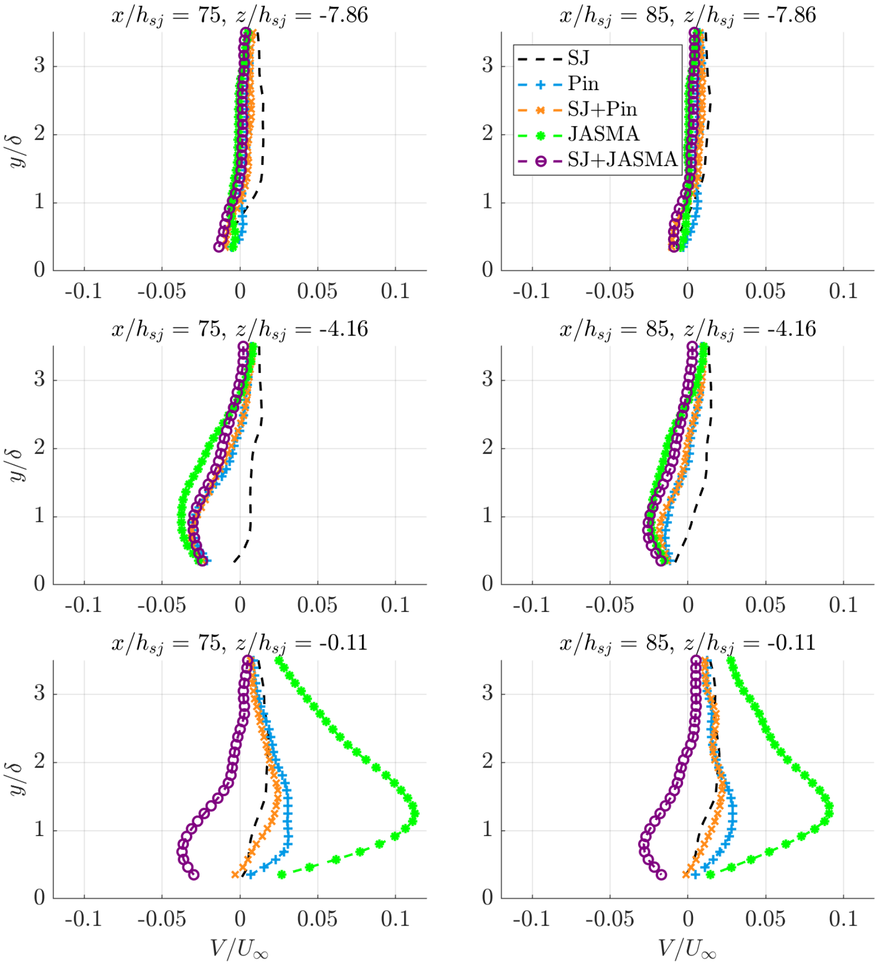

(b)

Fig. 11 (a) Schematic representation of the experimental setup with data domain in green and profile locations shown by the black dots. (b) Normalized vertical velocity profiles at six locations in the wake.

Finally, TKE color contours at the previous two streamwise stations are shown in Figure 12 for the five cases discussed prior. The TKE field due to the synthetic jet exhibits concentrations of TKE in regions resembling the vortical structures. However, all other cases add significant TKE to the flow comparatively. The SJ+pin case decreases the TKE compared to the pin-alone case. This suggests that much of the TKE introduced by the static pin is associated with the unsteadiness from the shear layer and the arch vortex, which are affected by the interaction with the SJ-generated hairpins. Since the frequency associated with the hairpins is different than the characteristic frequencies associated with the pin, they detract from this TKE. Moreover, the separated region behind the pin is reduced, leading to lower TKE. The JASMA tempers the TKE amplitudes from the pin-alone case, but its effect extends further above the plate by 0.5 to

1 boundary layer thicknesses. When the SJ and the JASMA are present together in the flowfield, the TKE is redistributed across the span of the domain for $z^* > 0$. Overall, these results confirm that the control schemes accomplish the purpose of this work, increasing mixing and momentum addition near the surface as compared to the laminar boundary layer with the hairpin train (the generation case). These results also suggest that further criteria for assessment of the control may be needed than TKE alone.

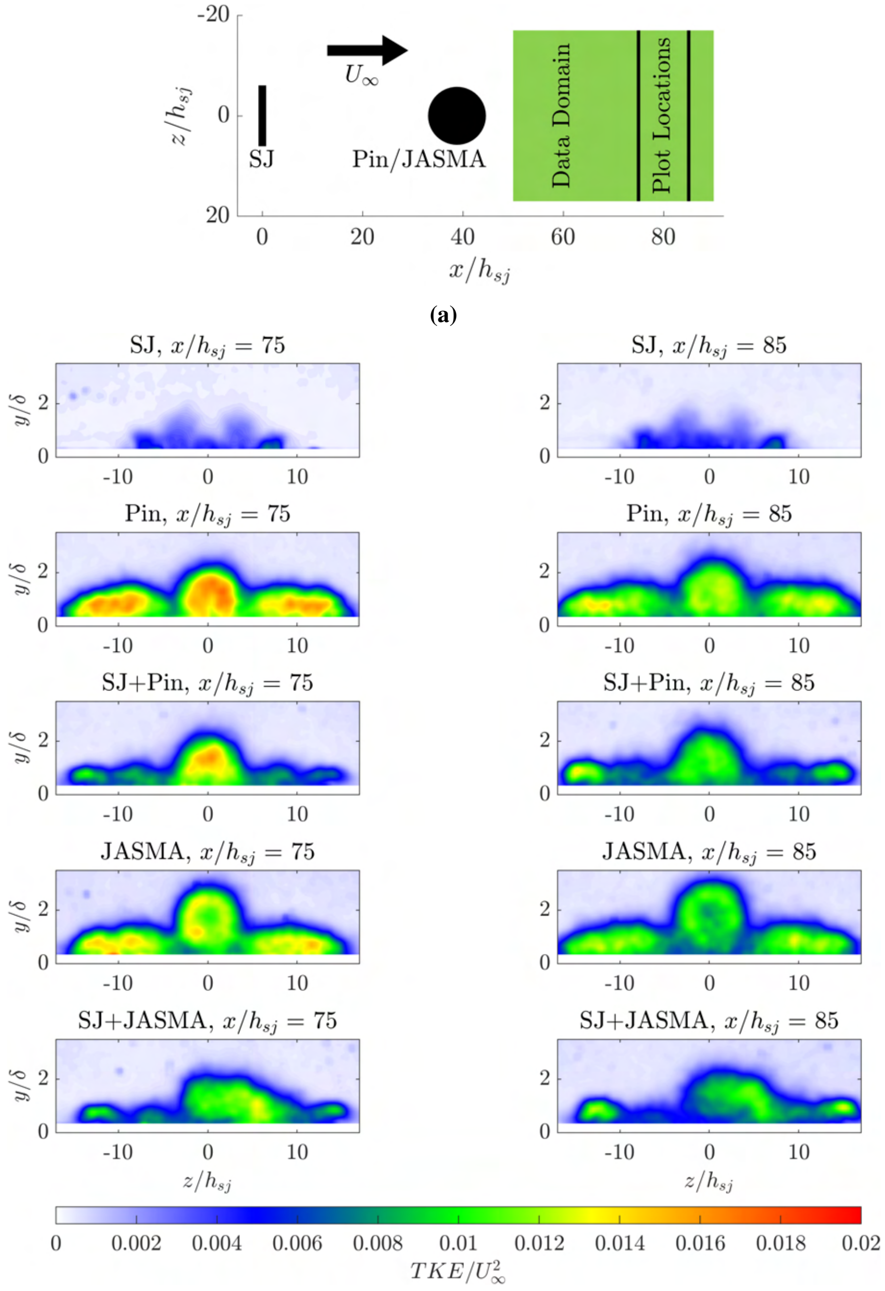

(a)

(b)

Fig. 12 (a) Schematic representation of the experimental setup with data domain in green and contour locations shown by the solid black lines. (b) Contours of normalized TKE at $x^* = 75$ (left column) and 85 (right column) for the SJ alone (row 1), static pin alone (row 2), SJ with static pin (row 3), JASMA alone (row 4), and SJ with JASMA control (row 5). Flow is into the page.

V. Conclusion and Future Work

The effect of passive and active devices on an artificially generated train of hairpin vortices in a laminar boundary layer was explored experimentally. Planar and stereoscopic PIV measurements were acquired for several configurations of generation and control of the hairpin vortices. Planar measurements were used to narrow the parameter space for variables such as synthetic jet and JASMA pitch angles (α_{sj} and γ), synthetic jet and JASMA blowing ratios ($C_{b_{sj}}$ and C_{b_J}), and pin height (h_p). A particular set of synthetic jet and pin/JASMA parameters was investigated using SPIV measurements in the wake of the pin. The results captured the evolution of the hairpin train and showed that they were not overly disrupted by the pin. It was found that the static pin and the JASMA introduced TKE to the flow due to actuation as well as increased downwash. Both of these outcomes are desirable for re-energizing separating flows.

Future work will investigate a finer tuning of the JASMA blowing ratio to better observe the effect on the SJ-generated hairpins for boundary layer re-energization because the JASMA-generated vortices are much larger than those of the SJ hairpins in the interaction domain. Additionally, the same control strategy must be assessed in a TBL where the LSMs naturally occur. Other work is in progress to use highly temporally resolved phase-locked data planes as inflow boundary conditions for direct numerical simulations. The simulations can be used to cut back on the experimental data collection time required to test the large parameter space for the synthetic jet generation case.

Acknowledgments

This work was funded under the National Science Foundation (award number 2129494) and monitored by Dr. Ron Joslin. The contributions of the collaborators for this grant at the University of Texas at Austin (Dr. David Goldstein, Dr. Efstathios Bakolas, Dr. Alexandros Tsolovikos, and Akshit Jariwala) and the University of Akron (Dr. Saikishan Suryanarayanan) are gratefully acknowledged. The authors would also like to thank Jasmine Narine for her help with model design for the wind tunnel experiments and Paul Remneff and Lilly Mertzlufft for their help with experimental data acquisition.

References

[1] Adrian, R. J., "Hairpin vortex organization in wall turbulence," *Physics of Fluids*, Vol. 19, No. 4, 2007, pp. 1–16. https://doi.org/10.1063/1.2717527.

[2] Guala, M., Hommema, S. E., and Adrian, R. J., "Large-scale and very-large-scale motions in turbulent pipe flow," *Journal of Fluid Mechanics*, Vol. 554, 2006, pp. 521–542. https://doi.org/10.1017/S0022112006008871.

[3] Hutchins, N., and Marusic, I., "Large-scale influences in near-wall turbulence," *Philosophical Transactions of the Royal Society A: Mathematical, Physical and Engineering Sciences*, Vol. 365, No. 1852, 2007, pp. 647–664. https://doi.org/10.1098/rsta.2006.1942.

[4] Robinson, S. K., "Coherent motions in the turbulent boundary layer," *Annual Review of Fluid Mechanics*, Vol. 23, 1991, p. 601. https://doi.org/10.1146/annurev.fl.23.010191.003125.

[5] Zhou, J., Adrian, R. J., and Balachandar, S., "Autogeneration of near-wall vortical structures in channel flow," *Physics of Fluids*, Vol. 8, No. 1, 1996, pp. 288–290. https://doi.org/10.1063/1.868838.

[6] Zhou, J., Adrian, R. J., Balachandar, S., and Kendall, T. M., "Mechanisms for generating coherent packets of hairpin vortices in channel flow," *Journal of Fluid Mechanics*, Vol. 387, 1999, pp. 353–396. https://doi.org/10.1017/S002211209900467X.

[7] Acarlar, M. S., and Smith, C. R., "A study of hairpin vortices in a laminar boundary layer. Part 1. Hairpin vortices generated by hemisphere protuberances," *J. Fluid Mech*, Vol. 175, 1987, pp. 1–41. https://doi.org/10.1017/S0022112087000272.

[8] Acarlar, M. S., and Smith, C. R., "A study of hairpin vortices in a laminar boundary layer. Part 2. Hairpin vortices generated by fluid injection," *Journal of Fluid Mechanics*, Vol. 175, 1987, pp. 43–83. https://doi.org/10.1017/S0022112087000284.

[9] Haidari, A. H., and Smith, C. R., "The generation and regeneration of single hairpin vortices," *Journal of Fluid Mechanics*, Vol. 277, 1994, pp. 135–162. https://doi.org/10.1017/S0022112094002715.

[10] Taira, K., and Colonius, T., "Three-dimensional flows around low-aspect-ratio flat-plate wings at low Reynolds numbers," *Journal of Fluid Mechanics*, Vol. 623, 2009, pp. 187–207. https://doi.org/10.1017/S0022112008005314.

[11] Suponitsky, V., Cohen, J., and Bar-Yoseph, P. Z., "The generation of streaks and hairpin vortices from a localized vortex disturbance embedded in unbounded uniform shear flow," *Journal of Fluid Mechanics*, Vol. 535, 2005, pp. 65–100. https://doi.org/10.1017/S0022112005004453.

[12] Van Buren, T., Leong, C. M., Whalen, E., and Amitay, M., “Impact of orifice orientation on a finite-span synthetic jet interaction with a crossflow,” *Physics of Fluids*, Vol. 28, No. 3, 2016. https://doi.org/10.1063/1.4943520.

[13] Jabbal, M., and Zhong, S., “The near wall effect of synthetic jets in a boundary layer,” *International Journal of Heat and Fluid Flow*, Vol. 29, 2008, pp. 119–130. https://doi.org/10.1016/j.ijheatfluidflow.2007.07.011.

[14] Straccia, J. C., and Farnsworth, J. A. N., “On the vortex dynamics of synthetic jet – turbulent boundary layer interactions,” 2022. arXiv:2205.07370 [physics.flu-dyn].

[15] Zhou, J., and Zhong, S., “Coherent structures produced by the interaction between synthetic jets and a laminar boundary layer and their surface shear stress patterns,” *Computers and Fluids*, Vol. 39, 2010, pp. 1296–1313. https://doi.org/10.1016/j.compfluid.2010.04.001.

[16] Johnston, C. R., and Wilson, D. J., “A Vortex Pair Model for Plume Downwash into Stack Wakes,” *Atmospheric Environment*, Vol. 31, 1997, pp. 13–20. https://doi.org/10.1016/S1352-2310(96)00157-4.

[17] Park, C. W., and Lee, S. J., “Free end effects on the near wake flow structure behind a finite circular cylinder,” *Journal of Wind Engineering and Industrial Aerodynamics*, Vol. 88, No. 2-3, 2000, pp. 231–246. https://doi.org/10.1016/S0167-6105(00)00051-9.

[18] Sumner, D., Heseltine, J. L., and Dansereau, O. J. P., “Wake structure of a finite circular cylinder of small aspect ratio,” *Experiments in Fluids*, Vol. 37, No. 5, 2004, pp. 720–730. https://doi.org/10.1007/s00348-004-0862-7.

[19] Gildersleeve, S., and Amitay, M., “Vortex dynamics of a low aspect ratio cantilevered cylinder immersed in a boundary layer,” *Journal of Fluid Mechanics*, Vol. 901, 2020. https://doi.org/10.1017/jfm.2020.555.

[20] Sakamoto, H., and Arie, M., “Vortex shedding from a rectangular prism and a circular cylinder placed vertically in a turbulent boundary layer,” *J. Fluid Mech*, Vol. 126, 1983, pp. 147–165. https://doi.org/10.1017/S0022112083000087.

[21] Kawamura, T., Hiwada, M., Hibino, T., Mabuchi, I., and Kumada, M., “Flow around a finite circular cylinder on a flat plate,” *Bulletin of the JSME*, 1984, pp. 2142–2151. https://doi.org/10.1299/jsme1958.27.2142.

[22] Spinosa, E., “Control of Near-Wall Coherent Structures in a Turbulent Boundary Layer Using Synthetic Jets,” Ph.D. thesis, University of Manchester, 2016.

[23] Amitay, M., and Gildersleeve, S., “Methods and apparatus for controlling flow fields,” March 2020, US Patent No.: US 2020/0072259.

[24] Gildersleeve, S., and Amitay, M., “Three-dimensional wake characteristics associated with the jet assisted surface mounted actuator,” *2018 AIAA AVIATION Forum*, American Institute of Aeronautics and Astronautics Inc, AIAA, 2018, pp. 1–14. https://doi.org/10.2514/6.2018-3060.

[25] Gildersleeve, S. M., “Fundamental investigation of the flow around a finite span low aspect ratio pin and its application to flow control,” Ph.D. thesis, Rensselaer Polytechnic Institute, 11 2018.

[26] Tsolovikos, A., Suryanarayanan, S., Bakolas, E., and Goldstein, D., “Model Predictive Control of Material Volumes with Application to Vortical Structures,” *AIAA Journal*, Vol. 59, 2021, pp. 4057–4070. https://doi.org/10.2514/1.j060413.

[27] Jariwala, A., Tsolovikos, A., Suryanarayanan, S., Bakolas, E., and Goldstein, D., “On the Effect of Manipulating Large Scale Motions in a Boundary Layer,” *AIAA AVIATION Forum*, 2022, pp. 1–12. https://doi.org/10.2514/6.2022-3771.

[28] Adrian, R. J., Meinhart, C. D., and Tomkins, C. D., “Vortex organization in the outer region of the turbulent boundary layer,” *Journal of Fluid Mechanics*, Vol. 422, 2000, pp. 1–54. https://doi.org/10.1017/S0022112000001580.

Appendix: Lists of Planar and Stereoscopic PIV Experiments

Table 1 List of 2D Test Cases

α_{sj} (°)	$C_{b_{sj}}$	h_p (mm)	γ (°)	C_{b_J}
45	0	0		
45	0.5	0		
45	1.0	0		
90	0	0		
90	0.5	0		
90	1.0	0		
45	0	2.0		0
45	0.5	2.0		0
45	0	3.0		0
45	0.5	3.0		0
45	1.0	3.0		0
45	0	3.0	0	0.5
45	0.5	3.0	0	0.5
45	0	3.0	20	1.0
45	0.5	3.0	20	1.0
45	1.0	3.0	20	1.0
45	0	3.0	20	0.5
45	0.5	3.0	20	0.5
90	0	3.0		0
90	0.5	3.0		0
90	0	3.0	0	1.0
90	0.5	3.0	0	1.0
90	0	3.0	20	1.0
90	0.5	3.0	20	1.0
90	0	4.0		0
90	0.5	4.0		0
90	1.0	4.0		0
90	0	4.0	20	1.0
90	0.5	4.0	20	1.0
90	1.0	4.0	20	1.0

Table 2 List of Volumetric Test Cases

α_{sj} (°)	$C_{b_{sj}}$	h_p (mm)	γ (°)	C_{b_J}	ϕ (°)
45	0	0			Baseline
45	0.5	0			TA
45	0.5	0			0
45	0.5	0			90
45	0.5	0			180
45	0.5	0			270
90	0	0			Baseline
90	0.5	0			TA
90	0.5	0			0
90	0.5	0			90
90	0.5	0			180
90	0.5	0			270
45	0	1.0			Baseline
45	0.5	1.0			TA
45	0.5	1.0			0
45	0.5	1.0			90
45	0.5	1.0			180
45	0.5	1.0			270
45	0	2.0			Baseline
45	0.5	2.0			TA
45	0.5	2.0			0
45	0.5	2.0			90
45	0.5	2.0			180
45	0.5	2.0			270
45	0	3.0	0	0	Baseline
45	0.5	3.0	0	0	TA
45	0.5	3.0	0	0	0
45	0.5	3.0	0	0	90
45	0.5	3.0	0	0	180
45	0.5	3.0	0	0	270
45	0	3.0	0	0.5	TA
45	0	3.0	0	0.5	0
45	0	3.0	0	0.5	90
45	0	3.0	0	0.5	180
45	0	3.0	0	0.5	270
45	0.5	3.0	0	0	TA
45	0.5	3.0	0	0	0
45	0.5	3.0	0	0	90
45	0.5	3.0	0	0	180
45	0.5	3.0	0	0	270